Available online at www.sciencedirect.com
ScienceDirect
Ceramics International 37 (2011) 2917–2920
CERAMICS INTERNATIONAL
www.elsevier.com/locate/ceramint

Short communication

Microemulsion process synthesis of lanthanide-doped hydroxyapatite nanoparticles under hydrothermal treatment

Yuxiu Sun [a,*], Hua Yang [a], Dongliang Tao [b]

[a] Department of Chemistry, Tianjin Normal University, Xiqing District Binshui West Road 393, Tianjin 300387, China
[b] College of chemistry and chemical engineering, Fuyang Normal College, Anhui 236041, China

Received 4 February 2011; received in revised form 17 March 2011; accepted 18 March 2011
Available online 1 April 2011

Abstract

Luminescent lanthanide-doped hydroxyapatites (Eu:HA and Eu–La:HA) were successfully fabricated via the (cyclohexane/polyxyethylene (TX-100)/*n*-butanol/water solution) microemulsion mediated hydrothermal process. The structure, morphology, and optical properties were systematically characterized by X-ray diffraction (XRD), transmission electron microscopy (TEM), and photoluminescence (PL) spectra, respectively. The XRD results reveal that the obtained Eu:HA and Eu–La:HA nanoparticles also show the characteristic peaks of hydroxyapatite in a hexagonal lattice structure. It is observed that the as-prepared luminescent samples exhibit sphere-like morphology with well dispersed and non-aggregated size distribution. Upon excitation by UV radiation, the Eu:HA samples demonstrate the characteristic $^5D_0$–$^7F_{1-4}$ emission lines of Eu^{3+}. Moreover, the PL emission intensity of Eu^{3+} can be tuned by importing La^{3+} ions into the structure of europium-doped hydroxyapatite nanocrystals within some Eu^{3+}:La^{3+} doping contents, and altering the doping concentration of Eu^{3+}.

Keywords: Hydroxyapatite; Lanthanide; Luminescence; Microemulsion; Hydrothermal

1. Introduction

Hydroxyapatite [HA, $Ca_5(PO_4)_3(OH)$] has been widely used as a bone substitute due to its adequate mechanical properties and the similar composition to bone mineral [1,2]. Recently, a great number of substitutions, especially the composites resulting from the cationic substitution are of potential application in the fields of dental and bone pathologies, bioceramics, luminescence, water purification, and catalysis, because of the high stability and flexibility of the apatitic structure [3–7]. Moreover, compared with other rare earth ions, Eu^{3+} ions have simple electronic energy level scheme and hypersensitive transitions, and which have been utilized extensively in color television and high efficiency fluorescent lamps [8,9], and was also believed as a good candidate of biological probe because of its more stable luminescence with time in comparison with fluorescent organic molecules [10–12]. Therefore, hydroxyapatite with general formula $Ca_5(PO_4)_3(OH)$ was the nice host of Eu^{3+} doping since Eu^{3+} has a similar ionic radius to Ca^{2+} in hydroxyapatite.

So far, various techniques, such as chemical co-precipitation [13,14], sol–gel process [15,16], hydrothermal synthesis [17,18], emulsion and microemulsion [19–21], microwave irradiation [22,23], and microemulsion process under hydrothermal treatment [24] have been employed for the synthesis of hydroxyapatite. Among those synthesis methods, the combination of the hydrothermal synthesis with the reverse micelle process may provide a unique approach for the synthesis of HA particles with high crystallinity and special morphology. The products of hydrothermal–microemulsion reactions are usually crystalline and do not require post-annealing treatments. At the same time, the morphologies of the products can be controlled by the reverse microemulsion.

Although some lanthanide-doped hydroxyapatite nanoparticles have been synthesized through microemulsion process under hydrothermal treatment [25], the fluorescent properties of europium doped hydroxyapatite nanocrystallines with different doping concentrations have not been discussed and how some other ions affect the fluorescent intensity of europium doped HA have not been found yet. It is well accepted that the properties of HA are strictly linked to their nanoscale dimensions and morphologies [26,27], and the import of some other metal ions should increase the intensity of

* Corresponding author. Tel.: +86 22 23766516.
E-mail address: hxxysyx@mail.tjnu.edu.cn (Y. Sun).

0272-8842/$36.00
doi:10.1016/j.ceramint.2011.03.030

europium-doped HA luminescence property. Therefore, the design and development of luminescence functionalized HA with nano-sized and with some other metal ions coexistence should be able to reach this goal.

In this paper, we synthesize the Eu^{3+} doped, and Eu^{3+}–La^{3+} doped hydroxyapatite nanoparticles with uniform morphology and narrow size distribution, respectively, through a cyclohexane/polyxyethylene (TX-100)/*n*-butanol/water solution microemulsion process under hydrothermal treatment. The fluorescent properties of europium doped hydroxyapatite nanocrystallines with different doping concentration will be discussed briefly. Additionally, the influence factor such as the import of La^{3+} ion on the luminescence property of the Eu^{3+} doped hydroxyapatite nanoparticles will also be investigated as well.

2. Materials and methods

All the reagents were purchased without further purification. The doping concentration of Eu^{3+} was 0.5–5 mol% to Ca^{2+} in Eu:$Ca_5(PO_4)_3(OH)$ (Eu:HA), in which effect of Europium doping concentration on luminescent properties of Eu:HA will be found out. The molar ration of La^{3+}–Eu^{3+} was 0.5:1; 1:1; 2:1; 4:1 in Eu^{3+}–La^{3+} mixture ions doped hydroxyapatite nanoparticles (Eu–La:HA), and $Eu(NO_3)_3$ and $La(NO_3)_3$ were obtained by dissolving stoichiometric Eu_2O_3 and La_2O_3 in dilute HNO_3 with vigorous stirring, respectively. The superfluous HNO_3 was driven off until the $Eu(NO_3)_3$ and $La(NO_3)_3$ crystal powders were obtained. The reverse microemulsion was prepared according to the literature [24]. Typically, polyxyethylene (TX-100) was selected as surfactant with n-butanol as cosurfactant, and cyclohexane as the oil phase. The volume ratio of cyclohexane to surfactant was 7:2, and surfactant to cosurfactant was 8:3.

2.1. Synthesis of Eu^{3+}, and Eu^{3+}–La^{3+} doped hydroxyapatite

In a typical synthesis, 5 mL of 0.5 M Ca^{2+}–Eu^{3+} water solution was added to the mixture containing 28 mL of cyclohexane, 8 mL of TX-100, 3 mL of *n*-butanol. Then 5 mL of 0.3 M $(NH_4)_2HPO_4$ was added with intense stirring, and the pH value of the microemulsion was adjusted to 8–9 using ammonia. After stirred intensely for 30 min, the resulting mixture was then transferred into a 50 mL sealed Teflon autoclave and statically heated at 160 °C for 12 h. The finally products were separated from the reverse microemulsion solution by centrifugation. The precipitate was then washed several times with ethanol, followed by drying 70 °C in an oven. In this way, the europium doped hydroxyapatite was obtained, which was designated as Eu:HA. The molar ratios of $Eu^{3+}/(Eu^{3+} + Ca^{2+})$ was 0–5 mol% in the 0.5 M water solution, and (Eu + Ca)/P = 1.67.

Eu^{3+} and La^{3+} doping hydroxyapatite designated as Eu–La:HA was also prepared through the same process at 160 °C for 12 h. The molar ratios of (Eu + La + Ca)/P = 1.67.

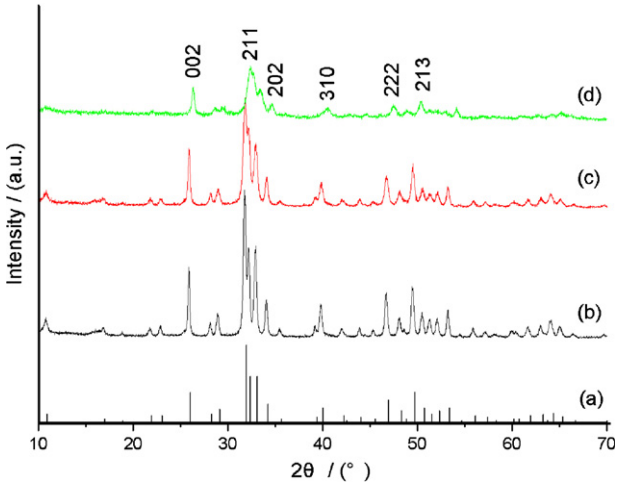

Fig. 1. XRD patterns of the standard data for hydroxyapatite (JCPDS No. 09-0432) (a); pure HA (b); Eu:HA ($Eu^{3+}/(Eu^{3+} + Ca^{2+})$ = 1%) (c) and Eu–La:HA (Eu:La = 1:2, $Eu^{3+}/(Eu^{3+} + Ca^{2+})$ = 1%) (d).

2.2. Characterization

Powder X-ray diffraction (XRD) patterns were obtained on a Rigaku diffractometer (D/Max 2500 V). The XRD data were recorded by using Cu Kα radiation (λ = 0.15406 nm) at a scanning rate of 15°/min in the 2θ range from 10° to 70°. The photoluminescence spectrum of the sample was recorded with a Hitachi F-4500 Fluorescence Spectrophotometer at room temperature. Transmission electron microscopy(TEM) images were recorded on a FEI Tecnai G2 S-Twin with an acceleration voltage of 200 kV.

3. Results and discussion

3.1. Structure, formation, morphology of pure HA, Eu:HA, and Eu–La:HA

Fig. 1 shows the XRD patterns of pure HA, Eu:HA, Eu–La:HA, and the standard data for the hexagonal hydroxyapatite, respectively. For pure HA Fig. 1b, the diffraction peaks can be well indexed to the hexagonal $Ca_5(PO_4)_3(OH)$ in $p6_3/m$ space group (JCPDS No. 09-0432). In the case of the Eu:HA and Eu–La:HA samples (Fig. 1c and d), the characteristic diffractions of hexagonal HA are still obvious, and no other metal oxide phases related with doped component can be detected. The calculated lattice constants of the above samples are compared with those of the JCPDS No. 09-0432 standard for hydroxyapatite. It shown that the calculated lattice constants of $a = b = 0.9416$ nm, $c = 0.6881$ nm for Eu:HA, and $a = b = 0.9408$ nm, $c = 0.6872$ nm for Eu–La:HA are in agreement with the standard data of $a = b = 0.9418$ nm, $c = 0.6884$ nm (space group $P6_3/m$). From the XRD patterns, it could also be seen that with the import of Eu^{3+} and La^{3+}, the intense diffraction peaks slightly decreased, indicating a small change in the crystalline structure leads to decline of ion-doped samples.

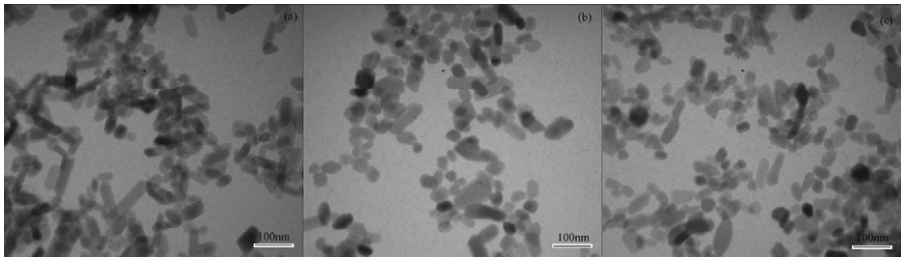

Fig. 2. TEM images of pure HA (a); Eu:HA ($Eu^{3+}/(Eu^{3+} + Ca^{2+}) = 1\%$) (b); Eu–La:HA (Eu:La = 1:2, $Eu^{3+}/(Eu^{3+} + Ca^{2+}) = 1\%$) (c), scar bar = 100 nm.

It is found that all the samples demonstrate a uniform sphere-like morphology, revealing that the doping components have little influence on the surface morphology of the samples (in Fig. 2). Fig. 2a shows the sphere like morphology with 24–50 nm in diameter, and few particles appear to be close to rod like shape, the other two rare earth ion doped samples in Fig. 2b and c are sphere like morphology with 25–50, 20–50 nm in diameter, respectively. Furthermore, the particle size along to a axis and along to *c* axis can also be received by importing the above XRD data into MID Jade 5.0 software, according to [0 0 2] crystal face ($2\theta = 25.88^\circ$) and [3 0 0] crystal face ($2\theta = 32.90^\circ$) diffraction peaks, respectively. It is evident that the particle size calculated from XRD tests (shown in Table 1) is in agreement with the results of TEM images within the error range.

XRD and TEM analysis suggest that microemulsion process under hydrothermal treatment can provide an effective process to obtain highly crystalline nanoparticles with mono-disperse and narrow size distribution. However, those results did not indicate that Eu^{3+} has been doped into the framework of HA, we could trace the doped rare earth ion in the structure of hydroxyapatite through PL spectra, since pure HA has no fluorescent property.

3.2. Effect of Europium doping concentration on luminescent properties of Eu:HA

In order to select the Eu doping content, the samples with different molar ratios (0.5%, 1% and 5%) of Eu/(Eu + Ca) were synthesized. The emission spectrum for the Eu:HA nanoparticles with different Eu doping contents were recorded at an excitation wavelength of 250 nm as shown in Fig. 3. These samples exhibit the two emission peaks at 592 and 617 nm, these emissions can be assigned to Eu $^5D_0$–$^7F_1$ and $^5D_0$–$^7F_2$ transitions respectively. We found that the PL intensity increased with the increase of the molar ratio of Eu/(Eu + Ca) to 0.5%, 1% and 5%, and no significant modification of emission spectra was observed.

Table 1
Particle size along to a axis and c axis of three samples.

Particle size\sample	Pure HA	Eu:HA	Eu–La:HA
a axis/nm	30.9	24.2	31.9
c axis/nm	59.6	37.2	34.6

3.3. Influence of La^{3+} on luminescent properties of Eu:HA

In order to investigate the influence of La^{3+} on luminescent properties of Eu:HA, four different Eu^{3+}:La^{3+} doping ratio samples were synthesized, which are Eu^{3+}:La^{3+} = 1:4; Eu^{3+}:La^{3+} = 1:2; Eu^{3+}:La^{3+} = 1:1 and Eu^{3+}:La^{3+} = 1:0.5. The emission spectrum for the Eu–La:HA samples between 560 and 700 nm was recorded at an excitation wavelength of 250 nm as

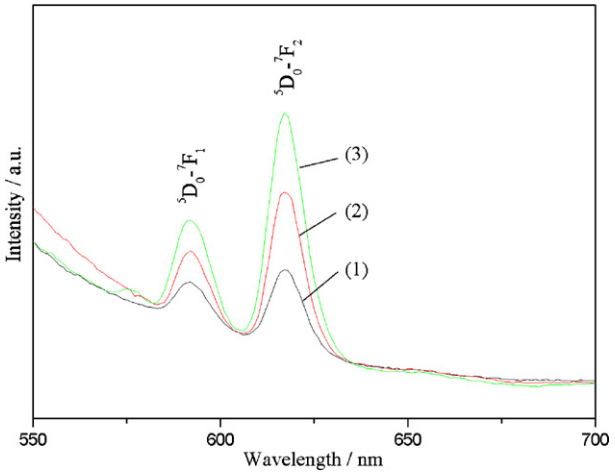

Fig. 3. Emission spectra of Eu:HA with different molar ratios Eu/(Eu + Ca) (λ_{ex} = 250 nm): (1) Eu^{3+} 0.5%; (2) Eu^{3+} 1% and (3) Eu^{3+} 5%.

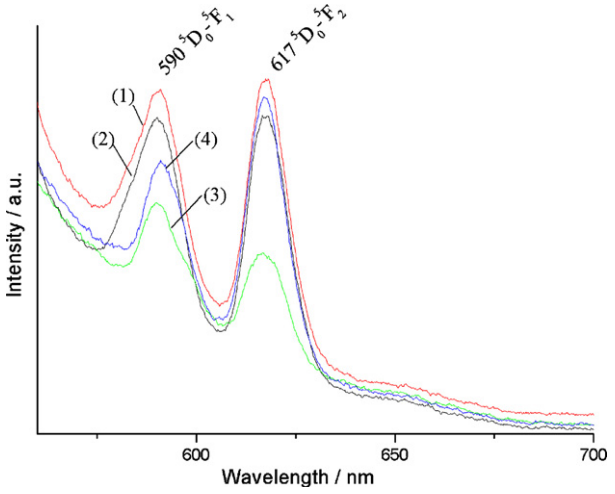

Fig. 4. Emission spectrum of HA samples with different Eu^{3+}:La^{3+} doping ratios under the excitation of 250 nm (1) Eu^{3+}:La^{3+} = 1:4; (2) Eu^{3+}:La^{3+} = 1:2; (3) Eu^{3+}:La^{3+} = 1:1 and (4) Eu^{3+}:La^{3+} = 1:0.5.

shown in Fig. 4. All samples exhibit two emissions maxima at 590 nm and 617 nm respectively. These two emission peaks can be assigned to Eu^{3+} $^5D_0$–$^7F_1$ (590 nm) and $^5D_0$–$^7F_2$ (617 nm), and the location of the emission lines with their assignments are labeled as well. From the spectra, we found that the location assigned to Eu^{3+} did not change with the doping of La^{3+} in to HA crystalline, and more interested is that the intensity of Eu^{3+} emission peak increased with the decrease of the ratio of Eu^{3+}–La^{3+} when Eu^{3+}:La^{3+} change from 1:4, 1:2, and 1:0.5, there existed minimum data when Eu^{3+}:La^{3+} = 1:1.

4. Conclusions

In summary, a feasible hydrothermal treatment assisted microemulsion process has been proposed to synthesize luminescent europium doped hydroxyapatite nanoparticles. The as-prepared Eu:HA nanoparticles shown are of high purity and crystallinity. PL intensity increased with the increase of the molar ratio of Eu/(Eu + Ca) to 0.5%, 1% and 5%, and no significant modification of emission spectra was observed. The photoluminescence intensities of the as-made Eu:HA nanoparticles can also be increased by importing La^{3+} ions into the structure of europium-doped hydroxyapatite nanocrystals, and the results indicate the intensity of Eu^{3+} emission peak increased with the decrease of the ratio of Eu^{3+} to La^{3+} when Eu^{3+}:La^{3+} change from 1:4, 1:2, and 1:0.5, there existed minimum data when Eu^{3+}:La^{3+} = 1:1.

Acknowledgements

This project is financially supported by the National Natural Science Foundation of China (NSFC 20803052), Doctoral Program Foundation of Tianjin Normal University of China (52X09007, 52LX31).

References

[1] L.L. Hench, J. Wilson, Surface-active biomaterials, Science 226 (1984) 630–636.
[2] W. Suchanek, M. Yoshimura, Processing and properties of hydroxyapatitebased biomaterials for use as hard tissue replacement implants, J. Mater. Res. 13 (1998) 94–117.
[3] Y. Matsumura, S. Sugiyama, H.J.B. Hayashi, J.B. Moffat, Lead–calcium hydroxyapatite: cation effects in the oxidative coupling of methane, J. Solid State Chem. 114 (1995) 138–145.
[4] E. Boanini, P. Torricelli, M. Gazzano, R. Giardinob, A. Bigi, Alendronate-hydroxyapatite nanocomposites and their interaction with osteoclasts and osteoblast-like cells, Biomaterials 29 (2008) 790–796.
[5] X. Chen, T. Wu, Q. Wang, J.W. Shen, Shield effect of silicate on adsorption of proteins onto silicon-doped hydroxyapatite (1 0 0) surface, Biomaterials 29 (2008) 2423–2432.
[6] J.K. Liu, Q.S. Wu, Y.P. Ding, Self-assembled synthesis and fluorescent modification of hydroxylapatite nanoribbons spheres, Eur. J. Inorg. Chem. (2005) 4145–4149.
[7] S. Sebti, R. Tahir, R. Nazih, A. Saber, S. Boulaajaj, Hydroxyapatite as a new solid support for the Knoevenagel reaction in heterogeneous media without solvent, Appl. Catal. A: Gen. 228 (2002) 155–159.
[8] R. Ternane, M. Trabelsi-Ayedi, N. Kbir-Ariguib, B. Piriou, Luminescence properties of Eu^{3+} in calcium hydroxyapatite, J. Lumin. 81 (1999) 165–170.
[9] A.A. Bol, A. Meijerink, Long-lived Mn^{2+} emission in nanocrystalline ZnS:Mn^{2+}, Phys. Rev. B 58 (1998) R15997–R16000.
[10] A. Doat, M. Fanjul, F. Pelle, E. Hollande, A. Lebugle, Europium-doped bioapatite: a new photostable biological probe, internalizable by human cells, Biomaterials 24 (2003) 3365–3371.
[11] A. Doat, F. Pelle, A. Lebugle, Europium-doped calcium pyrophosphates: allotropic forms and photo luminescent properties, J. Solid State Chem. 178 (2005) 2354–2362.
[12] A. Doat, F. Pelle, N. Gardant, A. Lebugle, Synthesis of luminescent bioapatite nanoparticles for utilization as a biological probe, J. Solid State Chem. 177 (2004) 1179–1187.
[13] S. Kannan, A.F. Lemos, J.M.F. Ferreira, Synthesis and mechanical performance of biological-like hydroxyapatites, Chem. Mater. 18 (2006) 2181–2186.
[14] R. Kumar, K.H. Prakash, P. Cheang, K.A. Khor, Temperature driven morphological changes of chemically precipitated hydroxyapatite nanoparticles, Langmuir 20 (2004) 5196–5200.
[15] A. Bigi, E. Boanini, K. Rubini, Hydroxyapatite gels and nanocrystals prepared through a sol–gel process, J. Solid State Chem. 177 (2004) 3092–3098.
[16] T.A. Kuriakosea, S.N. Kalkuraa, M. Palanichamyc, D. Arivuolid, K. Dierkse, G. Bocellif, C. Betzelb, Synthesis of stoichiometric nano crystalline hydroxyapatite by ethanol-based sol–gel technique at low temperature, J. Cryst. Growth 263 (2004) 517–523.
[17] S.N. Inés, V.K. Yury, I.L. Oleg, G. Van Tendeloo, S.G. Himadri, G. Francisco, Y. Masahiro, An effective morphology control of hydroxyapatite crystals via hydrothermal synthesis, Cryst. Growth Des. 9 (2009) 466–474.
[18] A.A. Chaudhry, S. Haque, S. Kellici, P. Boldrin, I. Rehman, F.A. Khalidc, J.A. Darr, Instant nano-hydroxyapatite: a continuous and rapid hydrothermal synthesis, Chem. Commun. 21 (2006) 2286–2288.
[19] M.J. Phillips, J.A. Darr, Z.B. Luklinska, I. Rehman, Synthesis and characterization of nano-biomaterials with potential osteological applications, J. Mater. Sci. Mater. Med. 14 (2003) 875–882.
[20] G.K. Lim, J. Wang, S.C. Ng, C.H. Chew, L.M. Gan, Processing of hydroxyapatite via microemulsion and emulsion routes, Biomaterials 18 (1997) 1433–1439.
[21] Y. Sun, G. Guo, Z. Wang, H. Guo, Synthesis of single-crystal HAP nanorods, Ceram. Int. 32 (2006) 951–954.
[22] A. López-Macipe, J. Gómez-Morales, R. Rodríguez-Clemente, Nanosized hydroxyapatite precipitation from homogeneous calcium/citrate/phosphate solutions using microwave and conventional heating, Adv. Mater. 10 (1998) 49–53.
[23] P. Parhi, A. Ramanan, A.R. Ray, Synthesis of nano-sized alkaline-earth hydroxyapatites through microwave assisted metathesis route, Mater. Lett. 60 (2006) 218–221.
[24] Y. Sun, G. Guo, D. Tao, Z. Wang, Reverse microemulsion-directed synthesis of hydroxyapatite nanoparticles under hydrothermal conditions, J. Phys. Chem. Solids 68 (2007) 373–377.
[25] C. Yang, P.P. Yang, W.X. Wang, J. Wang, M.L. Zhang, J. Lin, Solvothermal synthesis and characterization of Ln(Eu^{3+}, Tb^{3+})doped hydroxyapatite, J. Colloid Interface Sci. 328 (2008) 203–210.
[26] T.J. Webster, C. Ergun, R.H. Doremus, R.W. Siegel, R. Bizios, Enhanced functions of osteoblasts on nanophase ceramics, Biomaterials 21 (2000) 1803–1810.
[27] T.J. Webster, R.W. Siegel, R. Bizios, Enhanced surface and mechanical properties of nanophase ceramics to achieve orthopaedic/dental implant efficacy, Bioceramics 13 (2000) 321–324.